NINETEENTH EUROPEAN ROTORCRAFT FORUM

Paper No. G 6

PERIODIC MODEL-FOLLOWING CONTROLLER FOR THE INDEPENDENT MODAL CONTROL OF INDIVIDUAL BLADES USING SMART STRUCTURES

by

F. NITZSCHE

INSTITUT FÜR AEROELASTIK
GÖTTINGEN, GERMANY

September 14-16, 1993
CERNOBBIO (Como)
ITALY

ASSOCIAZIONE INDUSTRIE AEROSPAZIALI
ASSOCIAZIONE ITALIANA DI AERONAUTICA ED ASTRONAUTICA

Periodic Model-Following Controller for the Independent Modal Control of Individual Blades using Adaptive Materials

Fred Nitzsche*
DLR - Institut für Aeroelastik
Bunsenstr. 10, D-37073 Göttingen, FRG

Abstract

An Implicit Model-Following Controller is developed in the modal domain to attenuate the vibration characteristics of helicopter rotors using adaptive structures. The dynamics of the blade in the hover condition is taken as the reference model. The results indicate that the linearization of the elastic system in forward flight is achieved with relatively low control costs.

1. Introduction

The active control of rotary wing systems using the individual-blade-control (IBC) concept to achieve vibration reduction may be formulated under two different philosophies. According to the first, the aim is to reduce vibration by actuating in one individual blade in such a way that the *causes* of the phenomenon are suppressed: dynamic stall, shock, and vortex-blade interaction may be actively controlled by modifying the airfoil shape by either changing its camber or using a flap. Among the many actuators available, adaptive materials such as piezoelectric sheets or beams may be employed to respond to the variations of blade local pressure[1]. Since the knowledge of the *local* airflow characteristics is necessary, an excellent model of the rotor aerodynamics is obviously required to solve the problem[2].

Alternatively, the problem may be investigated under a more "aeroelastic approach" in which the *effects* caused by the same aerodynamic loads on the system's response are controlled. It was observed that the aeroelastic characteristics of an individual blade in the rotating frame strongly contributes to the vibration response of the entire rotor/fuselage system at certain frequencies[3]. These frequencies are located in the neighborhood of pN/rev, where p is an integer and N is the number of blades. In former studies, adaptive materials were employed to construct sensor/actuator distributed arrangements that were optimized to achieve *independent modal control* at a determined rotor advance ratio and blade azimuth position[4,5]. The approach is feasible if fast, adaptive, closed-loop controllers are employed to cope with the variations of the system's aeroelastic characteristics with the azimuth angle in *real time*. Nevertheless, the approach requires less sophisticated aerodynamic models of the rotor since only *global* parameters are used in the controller's synthesis. The intrinsic assumption is that the cause of higher blade response at certain frequencies is related to lower modal damping in the rotating frame.

The damping of an individual blade mode can be artificially increased by a closed-loop feedback controller for which the input is an electrical signal proportional to the blade's modal deformation. The signal may be generated by *sensors* made of embedded sheets of piezoelectric material. However, the lack of power and/or bandwidth associated with the available adaptive materials remains a problem to use them as *actuators*. An efficient control upon the blade loads developed in the helicopter forward

*Scientist. Member AIAA.

flight can only be achieved if more efficient adaptive materials become available[5-8].

The present paper extends the previous works that were dedicated to investigate the feasibility of using adaptive materials in the vibration control of rotary wings in forward flight. In these studies, the periodic aerodynamic loads were linearized at a determined azimuth position of the blade[5,7,9-10]. This assumption allowed the aeroelastic equations of motion to become partial differential equations with constant coefficients, and the simple tools from the Optimum Control Theory could be employed in the controller's synthesis. As a result, fast, real-time, but also very demanding controller characteristics were necessary to cope with the variations of the aeroelastic modes with respect to the azimuth angle. Extra modal damping can only be provided at very low control costs which result in saturation of the adaptive material[5]. It is expected that a controller which is intrinsically periodic can be less demanding on the adaptive material properties since it can actuate during an entire revolution of the blade. In the present paper, this procedure is accomplished by using the Model-Following Technique, which has been studied by several authors[11-14], extended to periodic systems by Nishimura[11], and particularly applied to rotary wings by McKillip[13-14].

2.Periodic Model-Following Modal Controller

The mathematical model of a single rotating blade including only the elastic flatwise bending (slope φ) and torsion (angle θ) degrees of freedom was developed in previous works[7,10]. The aeroelastic dimensionless differential equations of the open-loop system with a single input E_3 (voltage applied through the electrodes of a piezoelectric material divided by the saturation voltage E^*) are integrated in space by the integrating-matrix method, resulting in a system of 4n first-order equations in the time domain (n is the number of discretizing points taken along the blade).

$$\mathbf{F}\,\dot{\mathbf{x}} + \mathbf{G}\,\mathbf{x} = \mathbf{H}\,E_3, \tag{1}$$

where

$$\mathbf{F} = \begin{bmatrix} -\gamma I_b L_2 A_1 & L_2 A_2 \\ I_{2n} & 0_{2n} \end{bmatrix} \tag{2}$$

$$\mathbf{G} = \begin{bmatrix} -\nu^{-1} I_{2n} - L_1 Z + \gamma I_b L_2 A_0 & 0_{2n} \\ 0_{2n} & I_{2n} \end{bmatrix} \tag{3}$$

$$\mathbf{H} = \begin{bmatrix} -L_3 h \\ 0_{2n\times 1} \end{bmatrix} \tag{4}$$

$$\mathbf{x} = \begin{bmatrix} q & \dot{q} \end{bmatrix}^T \tag{5}$$

$$\mathbf{q} = \begin{bmatrix} [\varphi]_{1\times n} & [\theta]_{1\times n} \end{bmatrix}^T. \tag{6}$$

The matrices $\mathbf{L}_1$, $\mathbf{L}_2$ and $\mathbf{L}_3$ in Eqs. 2-4 (which are closely related to the "basic", n×n,

integrating matrix **L**) are defined according to the selected boundary conditions[7,10]. Integrating matrices provide a semianalytical closed solution to the problem. All terms of Eq. 1 are treated collectively, without the need of approximations such as the one introduced by the modal superposition method. In the previous equations, $\nu = m_R\Omega^2R^4/(EI)_R$ is a rotation parameter, γ is the Lock number, I_b is the total moment of inertia of the blade in flapping, and **1** and **0** are the unit and null matrices, respectively, with the dimensions in subscript. Matrix $\mathbf{A}_2$ contains the system's inertia parameters, Matrix **Z** the geometric stiffening terms, matrices $\mathbf{A}_0$ and $\mathbf{A}_1$ the aerodynamic coefficients (dependent on the advance ratio μ and the azimuth angle $\psi = \Omega t$), and Vector **h** the actuator's geometric and adaptive material characteristics. As opposed to the previous works[7,10], here the dimensionless time is counted in blade *revs*, $t = \psi/(2\pi)$, in order to set the fundamental period equal to one.

Next, Eq. 1 may be transformed into the corresponding modal form using bi-orthogonal relationships among the left and right complex eigenvectors of the non-self-adjoint system *at a fixed* μ *and* ψ (Eq. 7a-b):

$$\mathbf{x} = \mathbf{U}_r\,\eta; \qquad \eta = \mathbf{U}_l\,\mathbf{x} \tag{7a}$$

$$\mathbf{U}_l\mathbf{U}_r = \mathbf{1}_m; \qquad \mathbf{U}_l\mathbf{A}\,\mathbf{U}_r = {}'\Lambda^{-1}, \tag{7b}$$

where

$$\mathbf{A} = \begin{bmatrix} \mathbf{G}_{11}^{-1}\mathbf{F}_{11} & \mathbf{G}_{11}^{-1}\mathbf{F}_{12} \\ \mathbf{1}_{2n} & \mathbf{0}_{2n} \end{bmatrix}. \tag{8}$$

Therefore,

$$\dot{\eta} = {}'\Lambda\,\eta + \mathcal{B}\,\mathrm{E}_3, \tag{9}$$

where

$$\mathcal{B} = {}'\Lambda^{-1}\mathbf{U}_l\mathbf{B}, \tag{10}$$

and $'\Lambda$ is the matrix of complex-conjugate eigenvalues - the superscript $'(\ )$ represents a diagonal matrix - and $\mathbf{U}_r$ and $\mathbf{U}_l$ are the "right" and "left" modal matrices, respectively. If the nonlinear terms are included, the modal decomposition must be performed *at each instant of time*, and Eqs. 9-10 take a more general form:

$$\dot{\eta} = \mathcal{A}(t)\,\eta + \mathcal{B}(t)\,\mathrm{E}_3, \tag{9a}$$

$$\mathcal{B}(t) = \mathcal{A}^{-1}\mathbf{U}_l\mathbf{B}(t). \tag{10a}$$

The Model-Following technique is extended in the present work to complex-coefficient systems such as the one represented by the non-linear, periodic, differential equations which govern the amplitude displacements of the aeroelastic modes of a single blade in the rotating frame (Eqs. 9a-10a). In the forward flight the complex coefficients change from one azimuth angle to another and, hence, the modes themselves change their characteristics (frequency and damping). Since the non-linearity of the system is basically generated by the aerodynamics at $\mu \neq 0$,

$$F_\beta^\bullet = -(r^2 + \mu\, r\, \sin\psi)/2 \tag{11a}$$

$$F_\beta = -(\mu\, r\, \cos\psi + \mu^2 \sin\psi\, \cos\psi)/2 \tag{11b}$$

$$F_\theta = (r^2 + 2\mu\ r\ \sin\psi + \mu^2\sin^2\psi)/2, \tag{11c}$$

the "hover modes" ($\mu = 0$) are invariant (in Eqs. 11a-c, r is the radial coordinate, $F_\beta^\bullet$, F_β and F_θ are the unsteady aerodynamic coefficients). Therefore, the latter modes seem to be a natural choice to use as a basis for the modal decomposition. They also represent a good dynamic "reference" for the Model-Following technique because it is well-known that the hover condition is characterized by low rotor vibration. For this reason, the periodic nature of the *elastic* system may be considered a nuisance, a characteristic which could be eliminated or at least reduced through the feedback control. The Model-Following to be pursued in the present investigation is formulated to penalize the difference between the time derivatives of the "actual" modal state vector $\dot{\eta}$ (Eq. 9a) and the model

$$\dot{\eta}_m = {}'\Lambda\ \eta, \tag{12}$$

where ${}'\Lambda$ collects the complex eigenvalues of the blade at the hover condition. Note that this is an *implicit* formulation because the model response η_m is constructed using the actual system's state η. Therefore, the cost function penalizing the deviation of the actual blade dynamics in the forward flight from its hover (and linear) condition is

$$J = 1/2 \int_0^\infty \left[(\dot{\eta}-\dot{\eta}_m)^H \mathbf{Q} (\dot{\eta}-\dot{\eta}_m) + \rho E_3^2\right] dt, \tag{13}$$

where $\mathbf{Q}$ is a weighting matrix and the superscript H stands for the Hermitian transpose. This representation assumes that a full-state feedback is available. Alternatively, a regulator driven by the current generated through the electrodes of a sensor made from piezoelectric material may be used (Fig. 1). The output current is proportional to the modal amplitude:

$$\iota = \mathbf{C}\ \mathbf{x} = \mathbf{C}\ \mathbf{U}_r\ \eta = \mathcal{C}\ \eta. \tag{14}$$

Likewise for the model:

$$\iota_m = \mathcal{C}\ \eta_m. \tag{15}$$

Substitution of Eqs. 14 and 15 into Eq. 13 yields a cost function that penalizes the time derivative of the output current generated in forward flight from the current that would be generated in the hover condition. The expression resembles Eq. 13, replacing η and η_m by ι and ι_m, respectively, and noting that the weighting matrix has now a determined character:

$$\mathbf{Q} = \mathcal{C}^H\mathcal{C}. \tag{16}$$

The only design parameter in Eq. 13 becomes the scalar ρ, which represents the relative cost of the controller output to linearize the blade dynamic response characteristics.

Following the steps of McKillip's derivations[13-14], Eqs. 9a and 12 are substituted in Eq. 13, yielding:

$$J = 1/2 \int_0^\infty \left[\eta^H \mathbf{W}_{\eta\eta}\eta + 2\eta^H \mathbf{W}_{\eta E} E_3 + W_{EE} E_3^2\right] dt, \tag{17}$$

where

$$W_{\eta\eta} = (\mathcal{A} - \Lambda)^H Q (\mathcal{A} - \Lambda) \tag{18a}$$

$$W_{EE} = (\rho + \mathcal{B}^H Q \mathcal{B}) \tag{18b}$$

$$W_{\eta E} = (\mathcal{A} - \Lambda)^H Q \mathcal{B}. \tag{18c}$$

The optimum control problem is governed by the time-varying Riccati equation[14],

$$-\dot{P} = P \mathcal{D} + \mathcal{D}^H P - P \mathcal{E} P + \mathcal{F}, \tag{19}$$

where

$$\mathcal{D} = \mathcal{A} - (1/W_{EE}) \mathcal{B} W_{\eta E}^H \tag{20a}$$

$$\mathcal{E} = (1/W_{EE}) \mathcal{B} \mathcal{B}^H \tag{20b}$$

$$\mathcal{F} = W_{\eta\eta} - (1/W_{EE}) W_{\eta E} W_{\eta E}^H. \tag{20c}$$

Nishimura[11] determined that the periodic solution of Eq. 19 may be obtained by spectral factorization. It is necessary to compute the state transition matrix defined by:

$$d\Phi/dt = \mathbb{U}(t) \Phi(t,s) \tag{21}$$

with

$$\Phi(s,s) = 1; \qquad 1 \geq t \geq s \geq 0, \tag{22}$$

where the matrix $\mathbb{U}$ is constructed appending the system's direct η and adjoint $\chi = P \eta$ states (note that here the fundamental period is one).

$$\mathbb{U} = \begin{bmatrix} \mathcal{D} & -\mathcal{E} \\ -\mathcal{F} & -\mathcal{D}^H \end{bmatrix} \tag{23}$$

The solution starts by obtaining the fundamental transition matrix of Eq. 21, $\Phi(1,0)$. Next, the eigenvalues $\lambda_k = \alpha_k + i\omega_k$ and the corresponding eigenvectors Ψ_k of the fundamental transition matrix are computed and grouped according to stable λ^s and unstable λ^u modes, as determined by the real parts of α_k ($\alpha_k < 0$ corresponds to a stable mode).

$$\alpha_k = \ell n |\lambda_k| \tag{24a}$$

$$\omega_k = \tan^{-1}[\mathrm{Im}(\lambda_k)/\mathrm{Re}(\lambda_k)] \tag{24b}$$

The fundamental transition matrix is then factored as:

$$\Phi(1,0) = \begin{bmatrix} \Psi_{11} & \Psi_{12} \\ \Psi_{21} & \Psi_{22} \end{bmatrix} \begin{bmatrix} \Lambda[\lambda^s] & \\ & \Lambda[\lambda^u] \end{bmatrix} \begin{bmatrix} \Psi_{11} & \Psi_{12} \\ \Psi_{21} & \Psi_{22} \end{bmatrix}^{-1}. \tag{25}$$

The periodic solution of the Riccati equation at any time instant is finally found according to

$$P(t)=[\Phi_{21}(t,0)\Psi_{11}+\Phi_{22}(t,0)\Psi_{21}]^{-1}[\Phi_{11}(t,0)\Psi_{11}+\Phi_{12}(t,0)\Psi_{21}], \tag{26}$$

where the columns of the transition matrices $\Phi(t,0)$ are arranged to match the same factorization provided for $\Phi(1,0)$. The closed-loop gain is also obtained at any time instant:

$$K(t) = (1/W_{EE})(W_{\eta E}^{H} + \mathcal{B}^{H}P(t)). \tag{27}$$

Hence, the input voltage generated by the periodic regulator is determined:

$$E_3(t)= -K(t)\ \eta. \tag{28}$$

Equation 28 is substituted into Eq. 9a, leading to the closed-loop system's equations of motion:

$$\dot{\eta} = [\mathcal{A}(t) - \mathcal{B}(t)\ K(t)]\ \eta \tag{29a}$$

$$\iota = \mathcal{C}\ \eta. \tag{29b}$$

3.Computation of the Transition Matrices

In the present work the transition matrices were determined using the integrating-matrix method. For a given periodic system,

$$\dot{\mathbf{y}} = \mathbb{U}(t)\ \mathbf{y}, \tag{30}$$

the solution $\mathbf{y}(t) = \mathbf{y}(t+T)$ may be expressed as[15]:

$$\mathbf{y}(t) = \left[\mathbf{y}^1(t)\ \mathbf{y}^2(t)\ \ldots\right]\left[\mathbf{y}_1(0)^T\ \mathbf{y}_2(0)^T\ \ldots\right]^T, \tag{31}$$

where $\mathbf{y}^1(t)$ is the solution of Eq. 30 for the initial conditions $\mathbf{y}_1(0) = 1$ and all remaining $\mathbf{y}_k(0) = 0$; $\mathbf{y}^2(t)$ is the solution for the initial conditions $\mathbf{y}_2(0) = 1$ and all remaining $\mathbf{y}_k(0) = 0$, etc. The matrix collecting these independent solutions (left-hand side of Eq. 31) is identified to the transition matrix $\Phi(t,0)$. In particular, at $t = T$ (the fundamental period) the fundamental transition matrix is obtained.

Thus, both the transition matrices and the fundamental transition matrix may be calculated by an algebraic expression (Eq. 32). $T = 1$ is mandatory because the integrating matrices are normalized for the unity interval. In Eq. 32 m is the number of states, and (n-1) is the number of time intervals in which the period is discretized.

$$[\Phi]_{(n.m)xm}= (1_{n.m}-L^{*}[\mathbb{U}]_{n.m})^{-1}\left[[y_1(0)]\ |\ [y_2(0)]\ |\ \ldots\right] \tag{32}$$

The individual transition matrices are obtained by successively collecting the rows of the discretized $[\Phi]$, which correspond to integrations from $t = 0$ up to $t \leq 1$. The discretized initial-condition vectors in Eq. 32 have the form

$$[y_k(0)]_{(m.n)x1} = \left[[0]_{1xn} \cdots [I]_{1xn} [0]_{1xn} \cdots \right]^T, \quad (33)$$

where the unit vector is at the k^{th} position. The matrix inversion must be performed just once since it is only dependent on the integrating-matrix operator $\mathbf{L}^*$ (a block-diagonal matrix composed of as many nxn $\mathbf{L}$'s as the number of states) and the discretized version of $\mathbb{U}$ (a matrix $[\mathbb{U}]$ for which each element is transformed into a diagonal nxn matrix of repeated values).

The method achieved outstanding performance in both accuracy and computation time if compared to a numerical integration of the system using a traditional Range-Kutta algorithm based on second and third order formulas. In a modal formulation the number of states is never very high, which makes the matrix inversion of Eq. 32 very attractive. The discretization level of $[\mathbb{U}]$ was considered satisfactory when the poles of $\Phi(1,0)$ kept the double symmetry around the origin in the complex plane. Figure 2 depicts an example where both a "good" and a "bad" convergence of the method were obtained. Whenever a "bad" convergence is achieved, it is surely improved by increasing either the order of the integrating polynomial which defines $\mathbf{L}$ or the number of time intervals. The former solution is always preferred since it does not cause an increase in the size of the matrices involved in the inversion.

4.Results:

The rotor parameters are shown in Table 1, and the aeroelastic modes at the hover condition are summarized in Table 2. These aeroelastic modes were used to perform the modal decomposition of Eqs. 7a-b at $\mu = 0.32$ and all discretized t within the fundamental period, determining the periodic matrices in Eqs. 9a-10a. They also characterize the reference model in Eq. 12. The integrating-matrix method was used to obtain both $\Phi(t,0)$ and an additional solution with the arbitrary initial condition $\eta(0) = 1_{mx1}$, which will serve as a reference value to evaluate the performance of the controller (m is the number of modes, including the complex-conjugates). The system has a transient behavior in superposition to its periodic characteristics, since no external command is incorporated into the blade dynamics.

In the first simulations a full-state feedback is assumed, with $\mathbf{Q} = 1_m$. Figures 3a-b depict the results using the first four complex-conjugate modes. Figure 3a shows the time evolution of both the output ι and the input E_3 when compared to the open-loop situation. It is clear that even at the lowest control cost ($\rho = 0$) the performance of the controller is satisfactory, not reaching values of E_3 beyond the saturation level. Figure 3b presents a plot of the gain vector components along the period, indicating that a periodic controller was synthesized. Figures 4a-b are equivalent to Figs. 3a-b, but including the first six aeroelastic modes. In Fig. 4a it is observed that the performance of the closed-loop system is not improved in terms of modal damping because a unity $\mathbf{Q}$ penalizes the relative performance of modes 3 and 4 in comparison to modes 5 and 6 which have a much lower damping ratio. As a result, E_3 achieves a fraction of its level in Fig. 3a. However, when the shape of the peaks of both plots in Fig. 5 are compared, it is clear that a much more linear response of the system was achieved with this type of controller.

Next, a modal filter, as introduced in a previous study[4], is employed. The adaptive material is shaped according to the shape functions of Fig. 6 in order to generate both a distributed actuator and a distributed sensor that can selectively control the modal amplitudes associated with modes 5 and 6 (considered critical at 4/rev for a four-blade rotor). Here, these shape functions represent optimal distributions of the adaptive material along the complete period because they are constructed using the invariant "hover modes". The performance of such a controller is depicted in Figs. 7 and

8. In Fig. 7 it can be observed that at a very low cost (ρ = 0.001) the saturation of the adaptive material is achieved, but the output response is greatly suppressed. In particular, the mode at 4/rev is entirely suppressed (Fig. 8). However, if the present levels of saturation of the adaptive material are compared to their counterparts found in a former study[5], it becomes clear that the periodic controller is much less demanding from the actuator's performance, and hence more suitable to be introduced in the so-called "smart" rotors.

Table 1: Rotor Parameters

definition	parameter	value	units	definition	parameter	value	units
number blades	N	4		moment of inertia	$I_b/(m_R R^3)$	.333	
rotor radius	R	4.926	m	blade chord	c/R	.0555	
rotor frequency	Ω	44.4	rad/s	aero center offset	x_a/c	.1	
bend compliance	$(EI)_R D^*_{11}/R$	$[1]_{nx1}$		blade thickness	t/c	.12	
bend/tors cmpl.	$(EI)_R D^*_{13}/R$	$[0]_{nx1}$		piezo coeff (axial)	e_{3x}(PZT)	12.16	C/m^2
tors compliance	$(EI)_R D^*_{33}/R$	$[1.756]_{nx1}$		piezo coeff (shear)	e_{3s}(PZT)	4.602	C/m^2
ref stiffness	$(EI)_R$	6.89×10^4	$N.m^2$	saturation field	E^*(PZT)†	381	V/m
mass	m/m_R	$[1]_{nx1}$		piezo coeff (axial)	e_{3x}(PVDF)	.05396	C/m^2
ref mass	m_R	5.5	kg/m	piezo coeff (shear)	e_{3s}(PVDF)	.01500	C/m^2
radius gyration	k_θ/R	$[.03]_{nx1}$		saturation field	E^*(PVDF)‡	6350	V/m
lift coeff	a	2π		distance btw layers	d_a/c	.09	
air density	ρ	1.225	kg/m^3	actuator thickness	t_a/c	.015	
Lock-number	γ	5.654		sensor distance ...	z_s/c	.06	
rotation param	ν	92.66		from blade midplane			

†actuator (PZT = piezoceramic adaptive material)

‡sensor (PVDF = piezopolymer adaptive material)

Table 2: Open-loop Aeroelastic Modes
(hover)

mode no.	ω/Ω	ξ/Ω	description
1	-1.0765	-.4043	*1st bending*
2	+1.0765	-.4043	*1st bending*
3	-3.3436	-.7213	*2nd bending*
4	+3.3436	-.7213	*2nd bending*
5	-4.4756	-.1346	*1st torsion*
6	+4.4756	-.1346	*1st torsion*

5. Conclusions

1) In the present study, periodic Model-Following controllers were synthesized, aiming at helicopter rotor vibration attenuation employing adaptive materials as both

sensors and actuators. The model used the blade's dynamics at the hover condition as the reference to be followed by the controller. Periodic gains were obtained, indicating that the approach leads to more feasible solutions in terms of control power requirements.

2) The results indicate that the periodic system approaches the linear system aeroelastic characteristics with relative low gains, These aeroelastic characteristics are recognized to be associated to lower levels of rotor vibration.

3) Integrating matrices were used to obtain the transition matrices of the numerical solution associated with the time-dependent Riccati equation. The method presented a superior performance when compared to more traditional step-by-step integration methods such as the Range-Kutta.

References

1. Hanagud, S., Prasad, J. V. R, Bowles, T. and Nagesh Babu, G. L., "Smart Structures in the Active Control of Blade Vortex Interaction," *17th European Rotorcraft Forum*, Berlin, FRG, September 24-27, 1991, Paper No. 75.
2. Geißler, W., "Numerical Investigation of Dynamic Stall on Oscillating Airfoils," *Proceedings International Forum on Aeroelasticity and Structural Dynamics 1991*, Aachen, FRG, June 3-5, 1991, Vol. 1, pp. 85-93.
3. Ham, N. D., "Helicopter Individual-Blade-Control Research at MIT 1977-1985," *Vertica*, Vol. 11, No. 1/2, 1987, pp. 109-122.
4. Nitzsche, F., "Modal Sensors and Actuators for Individual Blade Control," *Proceedings AIAA/ASME/ASCE/AHS/ASC 34th Structures, Structural Dynamics and Materials Conference*, La Jolla, CA, USA, April 19-21, 1993, pp. 3507-3516.
5. Nitzsche, F. and Breitbach, E. J., "Vibration Control of Rotary Wings Using Smart Structures," *Proceedings International Forum on Aeroelasticity and Structural Dynamics 1993*, Strasbourg, France, May 24-26, 1993, (to be published).
6. Spangler, R. L., Jr. and Hall, S. R., "Piezoelectric Actuators for Helicopter Rotor Control," *Proceedings AIAA/ASME/ASCE/AHS/ASC 31st Structures, Structural Dynamics and Materials Conference*, Long Beach, CA, USA, April 2-4, 1990, pp. 1589-1599.
7. Nitzsche, F. and Breitbach, E. J., "Individual Blade Control of Hinged Blades Using Smart Structures," *18th European Rotorcraft Forum*, Avignon, France, September 15-18, 1992, Paper No. E6.
8. Strehlow, H. and Rapp, H. "Smart Materials for Helicopter Rotor Active Control," *Proceedings AGARD/SMP Specialists' Meeting on Smart Structures for Aircraft and Spacecraft*, Lindau, FRG, October 5-7, 1992, Paper No. 5.
9. Nitzsche, F. and Breitbach, E. J., "The Smart Structures Technology in the Vibration Control of Helicopter Blades in Forward Flight," *Proceedings 1st European Conference on Smart Structures and Materials*, Glasgow, U.K., May 12-14, 1992, pp. 321-324.
10. Nitzsche, F. and Breitbach, E. J., "A Study on the Feasibility of Using Adaptive Structures in the Attenuation of the Vibration Characteristics of Rotary Wings," *Proceedings AIAA/ASME/ASCE/AHS/ASC 33rd Structures, Structural Dynamics and Materials Conference*, Dallas, TX, USA, April 13-15, 1992, pp. 1391-1402.
11. Nishimura, T., "Spectral Factorization in Periodically Time-Varying Systems and Application to Navigation Problems," *Journal Spacecraft*, Vol. 9, No. 7, July 1972, pp. 540-546.
12. Kreindler, E. and Rothschield, D., "Model-Following in Linear-Quadratic Optimization," *AIAA Journal*, Vol. 14, No. 7, July 1976, pp. 835-842.
13. McKillip, R. M., Jr., "Periodic Control of the Individual-Blade-Control Helicopter Rotor," *Vertica*, Vol. 9, No. 2, 1985, pp. 199-225.
14. McKillip, R. M., Jr. "Periodic Model-Following for the Control-Configured Helicopter," *Journal of the American Helicopter Society*, July 1991, pp. 4-12.
15. Digundji, J. and Wendell, J.H., "Some Analysis Methods for Rotating Systems with Periodic Coefficients," *AIAA Journal*, Vol. 21, No. 6, June 1983, pp. 890-897.

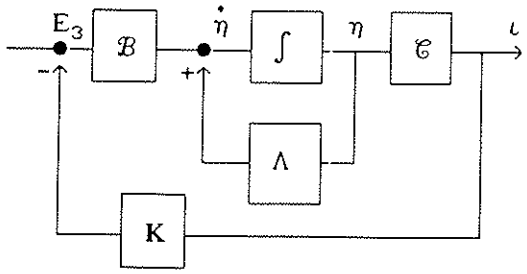

Fig.1 Single-Input-Single-Output Controller block-diagram.

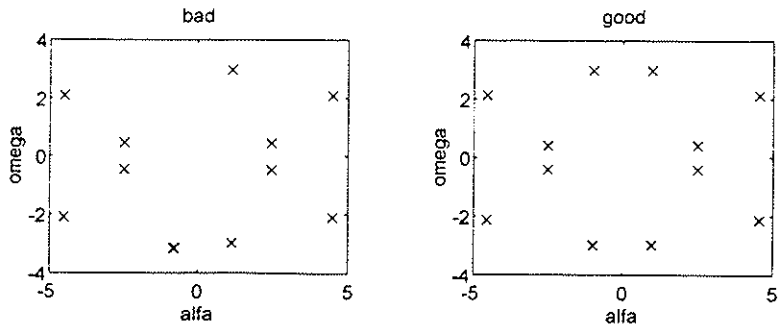

Fig.2 Fundamental Transition Matrix eigenvalues computed with the integrating matrix method: (left) "bad" convergence (n=20); (right) "good" convergence (n=30). Results obtained with a Newton, 7th order integrating matrix. Observe the double symmetry about the imaginary and real axis obtained with the "good" eigenvalues.

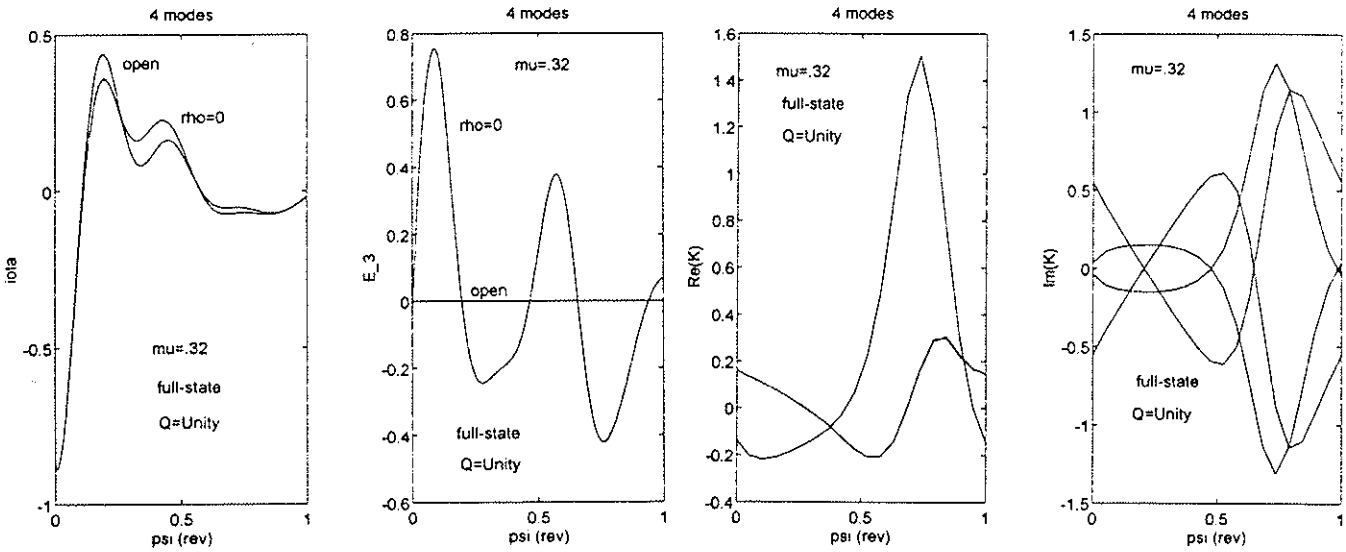

Fig.3 Periodic Modal-Following Modal Controller using 4 aeroelastic "hover modes" and **Q=I** (full-state feedback) for μ = 0.32: (3a) ι vs. ψ and E_3/E^* vs. ψ; (3b) Re(K) vs. ψ and Im(K) vs. ψ.

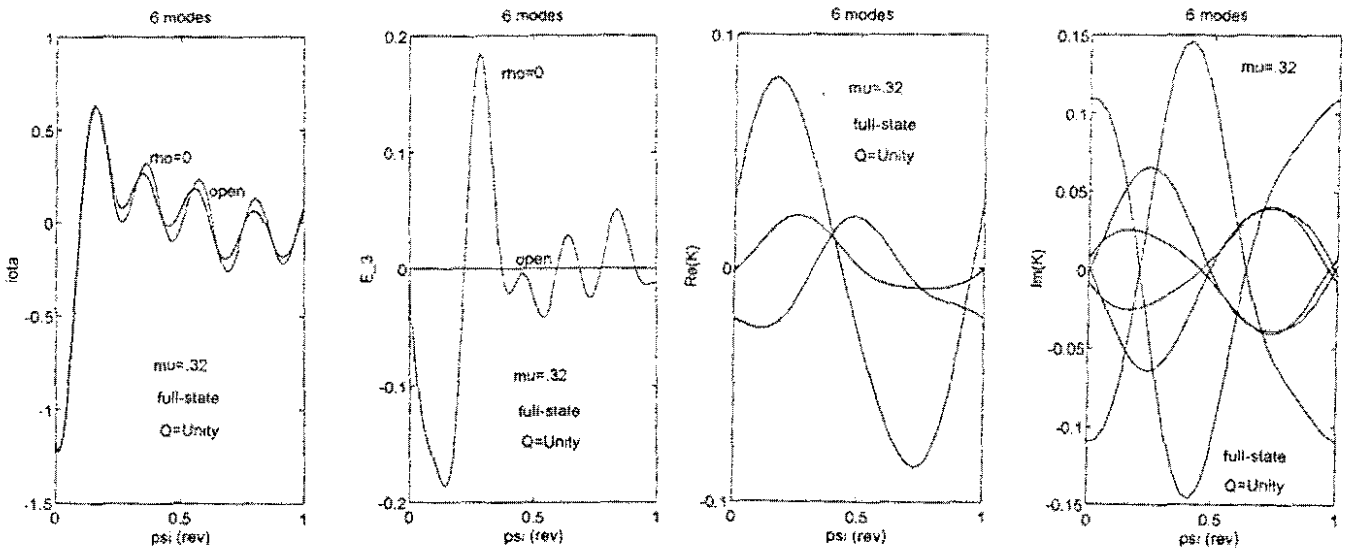

Fig.4 Periodic Modal-Following Modal Controller using 6 aeroelastic "hover modes" and **Q**=1 (full-state feedback) for μ = 0.32: (4a) ι vs. ψ and E_3/E^* vs. ψ; (4b) Re(K) vs. ψ and Im(K) vs. ψ.

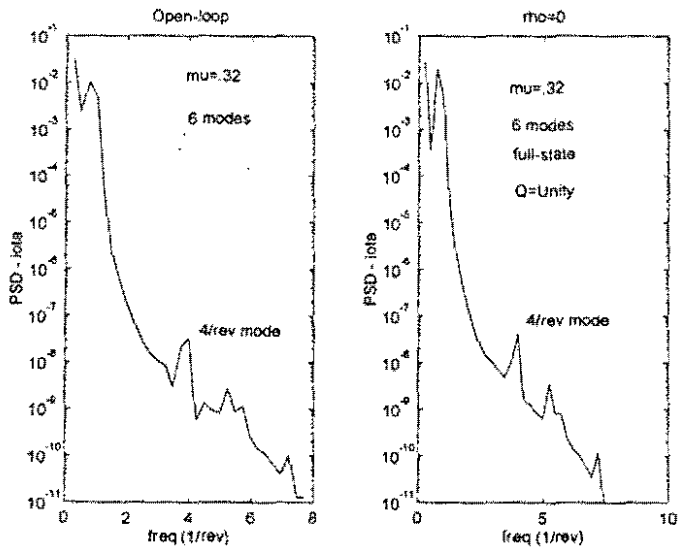

Fig.5 Power-Spectral-Densities of ι for the Open- and Closed-loop (ρ=0) systems for the 6-modes controller of Fig.4. The sharp peak of the 4/rev mode (right) indicates that the system presents a much more linear response with the controller on. The non-linear system behavior approaches the linear system behavior of the hover condition.

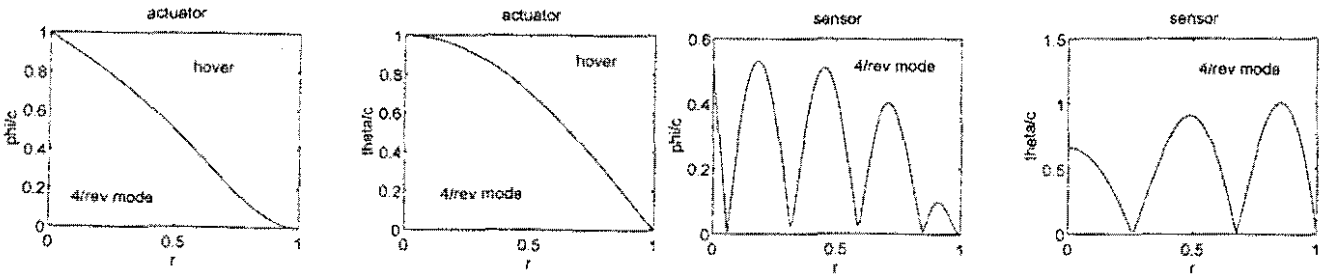

Fig.6 Modal filters[4] for the 4/rev mode. The four shape functions represent the width distribution (ϕ and θ) of the adaptive material along the blade: actuator (left), sensor (right): ϕ/c (bending component) vs. r and θ/c (torsion component) vs. r.

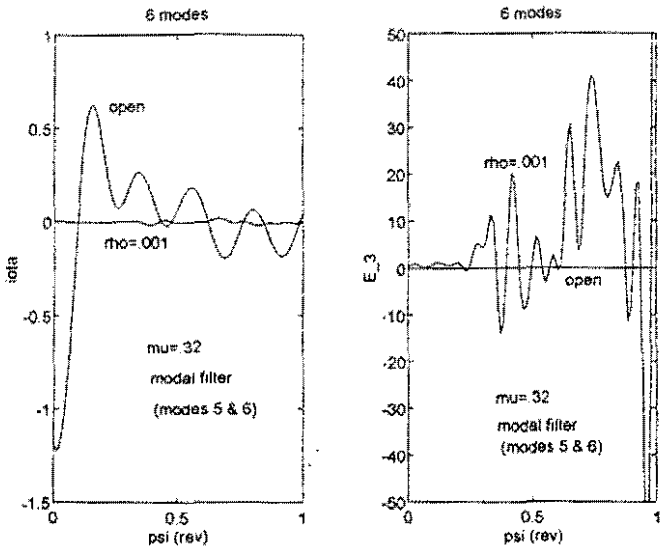

Fig.7 Periodic Modal-Following Modal Controller using 6 aeroelastic "hover modes" and $Q=\mathcal{C}^H\mathcal{C}$ (modal filters of Fig.6) for μ = 0.32: (left) ι vs. ψ and (right) E_3/E^* vs. ψ. Saturation of the adaptive material is reached for ρ=.001.

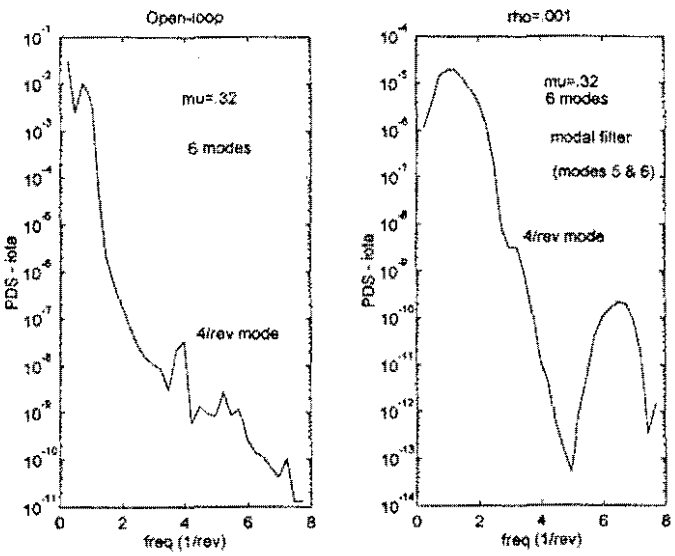

Fig.8 Power-Spectral-Densities of ι for the Open- and Closed-loop (ρ=.001) systems for the 6-modes controller of Fig.7. The 4/rev mode is completely suppressed using the modal filters of Fig.6.